Density of states and localization length in compositionally disordered quantum wires

K. Nikolić and A. MacKinnon
The Blackett Laboratory, Imperial College, Prince Consort Road, London SW7 2BZ, United Kingdom
(Received 21 August 1992)

Electronic states in compositionally disordered quantum wires are studied using a tight-binding Hamiltonian to determine the electronic density of states and localization lengths. The quantum wires are generated using the statistics of the structural roughness extracted from the results of computer simulations of molecular-beam-epitaxy growth of quantum-well wires on a vicinal surface. For monolayer structures, interface roughness and islands strongly suppress the subband structure. The electronic states are found to be localized to within several tens of lattice spacings, which implies severely reduced mobility in narrow quantum wires. Enlargement of the cross section of the wire by depositing additional layers does not improve the subband structure of the density of states. However, the localization lengths will be longer, except for energies near the band edge. The maximum localization length is proportional to the number of layers. Characteristic features of this model in the strong scattering regime, such as a spike in the density of states at the center of the subband and the gap around it, and strong reduction in the localization length for these energies, are observed for a monolayer structure. For multilayer structures spikes also occur at $E = \pm V$, but the gap has disappeared.

I. INTRODUCTION

In this paper we examine the effects of compositional disorder on the electronic density of states (DOS) and localization lengths of simulated quantum wires (structures where quantum confinement of carriers occurs in two dimensions). For this purpose we have used vicinal surface-grown quantum wires,[1,2] because only for the molecular-beam-epitaxy (MBE) growth process are sufficiently accurate details available. This enables one to perform Monte Carlo simulations of these wire structures and therefore, to define structural disorder in the system.[3,4] The effects of various types of compositional disorder considered here also have implications for the electronic behavior of quantum wires fabricated by other techniques.

The study of the electronic properties of semiconductor quantum wires is of interest not only for practical devices but also for a more fundamental research. Quantum wire structures have been predicted to have extremely high electron mobilities[5] due to strong suppression of both impurity and optical-phonon scattering. They also have features in the DOS which are very useful in laser applications, with the possibility of smaller current threshold density and better temperature stability[6] than in lasers produced from higher-dimensional structures. On the other side, quantum wires also provide a good model for studying electronic transport in ordered and disordered quasi-one-dimensional systems.

The MBE growth on slightly misoriented ($\sim 1°$–$4°$) surfaces (so-called *vicinal* surfaces) with submonolayer control over deposition has facilitated a new generation of very narrow (on a scale of a few nm) quantum wire structures. When a GaAs crystal is cut and polished with a small misorientation angle from a main crystallographic surface, in our case (100), the resulting surface consists of alternating steps and terraces. Then, appropriate fractional monolayers of AlAs and GaAs are alternately deposited by MBE. Under the correct conditions of flux and temperature, these adatoms are incorporated at the step edges.[2] Thus, growth takes place by step advancement and quantum wire structures are eventually obtained. The feasibility of this approach by using metal-organic chemical vapor deposition[7] (MOCVD) and migration-enhanced epitaxy[8] (MEE) has also been demonstrated.

However, the growth technique does not produce perfect wires. The interface between the GaAs and the AlAs regions is not smooth and, in addition, within the region of would be pure GaAs, there will inevitably be islands of AlAs. Even in two-dimensional (2D) heterostructures the interfaces can be imperfect since the growth front in MBE might be spread over several layers, which can influence some of the optical properties of quantum wells.[9] Disorder induced during the production of lateral confinement in quantum wires is usually stronger than in the epitaxial layer interface.

An important question is how compositional disorder affects the above-mentioned attractive features of quantum wires. Decreasing the lateral dimensions of the wires produces a wider separation of energy subbands but interface fluctuations become more important. Also in the quasi-one-dimensinal case there is a much higher probability of multiple scattering from the same site compared to the 2D or three-dimensional (3D) case. This could be in contradiction with the predicted extremely high mobility in quantum wires.

We suppose that the atoms of the wire are located at the sites of a simple cubic lattice. The one-electron tight-binding Hamiltonian for this system is given by

$$\mathbf{H} = \sum_i |i\rangle \varepsilon_i \langle i| + \sum_{\substack{i,j \\ (i \neq j)}} |i\rangle V_{ij} \langle j|, \tag{1}$$

where $|i\rangle$ is the s-state atomic orbital on a site i, ε_i is the "site energy," and V_{ij} is the hopping matrix element between sites i and j, which we shall assume to be zero unless the i and j sites are nearest neighbors, when $V_{ij} \equiv V = 1$ (i.e., V is a unit of energy). The Green's function of the system is defined by

$$\mathbf{G}(z) = (z\mathbf{I} - \mathbf{H})^{-1} . \tag{2}$$

The methods used in this work, and described below, attempt to exploit the nearest-neighbor features of the tight-binding Hamiltonian in the quasi-one-dimensional geometry. Also this model allows for an exact treatment of the disorder.

Here we simulate GaAs/AlAs wires, and therefore we choose $\varepsilon_{\mathrm{Al}} \gg \varepsilon_{\mathrm{Ga}}$. It has been shown[10] that, if $(\varepsilon_{\mathrm{Al}} - \varepsilon_{\mathrm{Ga}})/(2V) > 6$, then the spectrum of (1) splits into two subbands centered about $\varepsilon_{\mathrm{Ga}}$ and $\varepsilon_{\mathrm{Al}}$, respectively. Due to the high value of the Al site energy, off-diagonal disorder is not relevant. We have adopted $\varepsilon_{\mathrm{Ga}} = 0$. It is not our intention to describe a realistic GaAs/AlAs system in all detail, but rather to treat a system for which the scattering structure is similar to that of a realistic system.

II. DESCRIPTION OF THE QUANTUM WIRE STRUCTURE

The structure of the quantum wires examined here is obtained in the Monte Carlo simulations of AlAs/GaAs quantum wires grown on (100) vicinal surfaces by MBE.[1,2] Growth was simulated on a 120 × 80 lattice with four terrace steps each with a width of 20 lattice sites.[3] Wires are grown by alternately depositing the appropriate fraction of a monolayer of materials A, i.e., Al(As) and B, i.e., Ga(As) for a total of ten layers upon a substrate of material A. However, the growth simulations do not provide us with sufficiently long wires for the DOS and localization length calculations described below. Therefore we have developed an algorithm for quantum wire generation which enables us to deal with structures as long as we need (or equivalently, to create as big an ensemble as needed[11]). Firstly the structure of the wires from the growth simulations (Ref. 3) is analyzed and the form or compositional disorder extracted. Then arbitrarily long wires are generated with similar structural properties. Compositional disorder in the simulated structures is characterized by the wires' lateral edge (A/B interface) fluctuations and island structures of A atoms within the B wires, independently in each layer of the wire. The edge fluctuations and meandering are defined by the position of the center, $c = (y_r + y_l)/2$, and the width of the wire, $w = y_r - y_l$, for each slice along the wire (x direction). Here $y_r(x,z)$ and $y_l(x,z)$ are the positions of the left and the right edges of the wire, and z is the direction of the MBE growth.

Using this data for w and c, the probability distributions and two-point correlation functions were calculated for w, c, δw, and δc. This set of functions contains a large part of the information describing the systems from the growth simulations and an accurate reproduction of these distributions was taken as a requirement for a satisfactory generating algorithm. Sections of a simulated wire (as in Ref. 3) and a generated wire are given in Figs. 1(d) and 1(c), respectively. Since the generated wire is equivalent to the simulated one, i.e., to the real experimental wire, from now on we shall refer to it as a real wire. Furthermore, we are going to investigate the influence of different types of disorder separately, and therefore we are also treating real wire without islands [Fig. 1(b)], perfect wire (one with flat edges) with islands [Fig. 1(a)], and a meandering wire (wire with probability distributions of c and δc as for a real wire but with constant width). Most islands in this simulation are in fact single sites and the number of larger islands is satisfactorily reproduced by the probability of occurrence of several neighboring A atoms.[12]

We have also examined the effects of the number of layers in the wire on the electronic properties. Each layer in the wire is generated using the same statistics and correlations parameters. However, correlation between the layers is left as a functional parameter. We will examine three different levels of correlation between the layers.

(1) *Maximum correlation* is when the layers are identical. This means there is no disorder in the direction normal to the substrate surface.

(2) *Medium correlation* describes the case when corre-

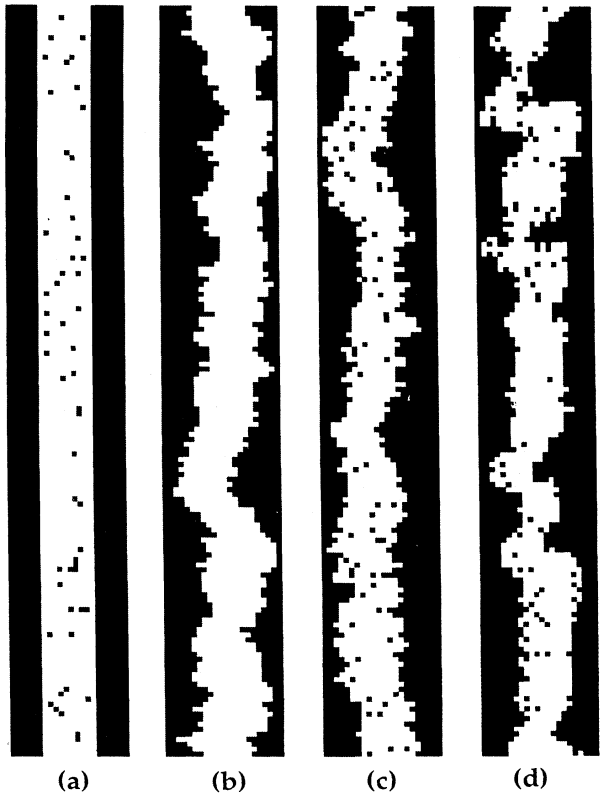

FIG. 1. Plot of sections of the monolayer quantum wires of average width ten: (a) perfect wire, with addition of islands, concentration $p = 0.05$; (b) real wire, without islands; (c) real wire, with island concentration $p = 0.05$; (d) as in the growth simulations (Refs. 3 and 4).

lation in the direction of growth (z) is identical to that along the wire (x). This can be achieved by sliding a layer for one slice, compared with the previous case of maximum correlation.

(3) *No correlation* is when layers are generated independently. This does not necessarily mean that all values for the difference in the positions of the lateral interfaces in the neighboring layers ($\Delta_z y$) are equally probable. The average width of the wire ($\langle w \rangle = 10$ or 15) is comparable to the total width of the system (that is the width of a terrace, typically 20), so smaller values for $\Delta_z y$ are more likely to occur than bigger.

In the simulations[3,4] quantum wire growth was modeled by considering a system where both constituent components A and B have identical kinetic properties. Therefore, the structure of any new deposited layer is completely independent of the structure of the previously grown layer. This leads us to the case of no compositional correlation between the layers. Nevertheless, not only for theoretical reasons, the other two cases are still interesting because, in reality, possible affinities between the same or different atoms cannot be completely ruled out.

III. DENSITY OF STATES

We shall first examine the influence of the islands of strongly scattering material on the DOS for the perfect wire (Sec. III A). Satisfactory results were obtained using the coherent-potential approximation (CPA) technique.[13] This approach enables us to carry out calculations for relatively large cross sections (e.g., 20×10) in an acceptable CPU time (roughly a few minutes on a CRAY X–MP/48 computer, per energy). Although this approximation cannot provide the small tails in the DOS diagram near the band edge, it is generally successful for this type of disorder because the islands are uncorrelated.

The edge roughness of the wire can also be treated by a similar technique, but only the generalized CPA method yields good results (see Ref. 13). If there is any correlation in the position of the edges at neighboring slices these generalizations become too complicated for our purpose. Therefore, in this case we have decided to rely on a numerical algorithm which counts eigenstates of the wire (Sec. III B).

A. Influence of the islands

Using the model of a perfect wire with islands [Fig. 1(c)] we have examined the effects of islands on the DOS. Calculations are done using the CPA with position-dependent self-energy. An outline of this method is given here. For a more detailed description see Ref. 13. The method uses the single-site CPA condition

$$\left\langle \frac{\varepsilon_i' - \sigma}{1 - (\varepsilon_i' - \sigma)\mathbf{G}_e(i,i)} \right\rangle_{\text{config}} = 0, \tag{3}$$

where $\varepsilon_i' = \varepsilon_i - \varepsilon_B$ and $\mathbf{G}_e = \langle \mathbf{G} \rangle_{\text{config}}$ is the Green's function of the effective wire. For $\varepsilon_A \to \infty$ and $\varepsilon_B = 0$, Eq. (3) gives the self-energy $\sigma(m)$ at the position m across the wire

$$\sigma(m) = -\frac{p_A(m)}{\mathbf{G}_e(m,m)}, \quad m = 1, 2, \ldots, M. \tag{4}$$

$p_A(m)$ is the probability of finding an A atom at position m in a cross section of the wire and M is the number of sites in a cross section. Using the concentration distribution across the wire $[p_A(m)]$ one is able to define some wire structures (like a perfect wire with islands), but the price is a position-dependent self-energy $\sigma(m)$ instead of a single scalar self-energy (as it is in the case of binary alloys). The $\mathbf{G}_e(m,m)$'s are the elements on the main diagonal of matrix $\mathbf{G}_d$, which corresponds to a slice of the effective wire, and by definition is the submatrix on the main diagonal of $\mathbf{G}_e$. For an infinite bar one has[14–16]

$$\mathbf{G}_d \equiv \mathbf{G}_d^{(\infty)} = \left[E\mathbf{I} - \mathbf{H}_e^{(1)} - 2\mathcal{V}^\dagger \mathbf{G}_d^{(\infty/2)} \mathcal{V}\right]^{-1}, \tag{5}$$

where $\mathbf{G}_d^{(\infty/2)}$ corresponds to a semi-infinite bar and is given by[15]

$$\mathbf{G}_d^{(\infty/2)} = \left[E\mathbf{I} - \mathbf{H}_e^{(1)} - \mathcal{V}^\dagger \mathbf{G}_d^{(\infty/2)} \mathcal{V}\right]^{-1}. \tag{6}$$

Here superscripts designate the length of the system. $\mathcal{V}$ contains the nearest-neighbor hopping elements between two slices. $\mathbf{H}_e^{(1)}$ is the Hamiltonian for an isolated effective slice, given by

$$\mathbf{H}_e^{(1)} = \sum_{m=1}^{M} |m\rangle \sigma(m) \langle m| + \sum_{m,n} |m\rangle \langle n|, \tag{7}$$

where the sites designated by labels m and n are nearest neighbors.

In the subband representation, i.e., in the basis of the eigenvectors of $\mathbf{H}_e^{(1)}$, the Green's function $\mathbf{G}_d$ is diagonal, with elements

$$g_i^{(\infty)}(E) = \pm \frac{1}{\sqrt{(E - e_i)^2 - 4}}, \quad i = 1, 2, \ldots, M, \tag{8}$$

where the e_i are the eigenvalues of $\mathbf{H}_e^{(1)}$. The sign of the square root is chosen so that $\mathrm{Im}(g_m^{(\infty)})$ and the DOS have the proper sign.[17]

The total DOS per site $\rho(E)$ is defined as

$$\rho(E) = \frac{-1}{\pi M} \mathrm{Im}\left[\mathrm{Tr}\mathbf{G}_d(E + \mathrm{i}0^+)\right]. \tag{9}$$

In order to calculate the DOS, the set of equations (4), (7), and (8) is iterated until self-consistency is achieved.

In Fig. 2 are presented the results of calculations for the perfect wire of width 10 with one, two, five, and ten layers and island concentration $p = 5\%$. The presence of the islands in the wire structures substantially degrades the (inverse square-root singularity) peaks of the DOS. The effect is similar in each subband of the wire. This is consistent with Eq. (4) for the self-energy, which is not dependent on the subband index.

If one multiplies the DOS per site by the number of

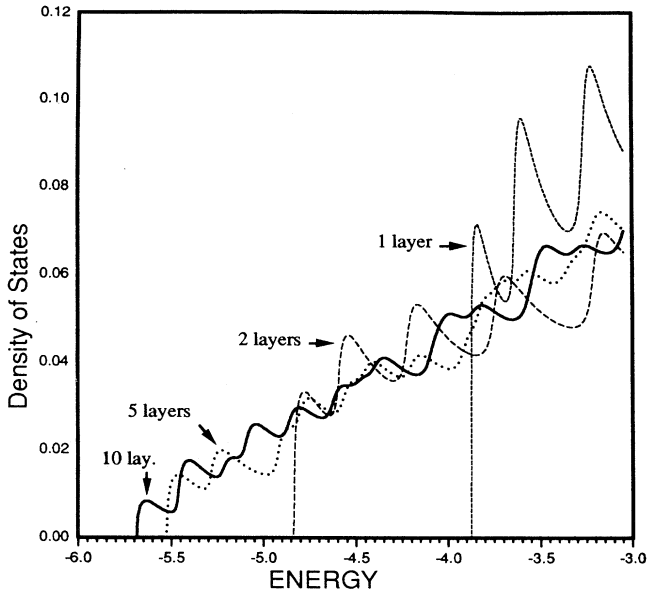

FIG. 2. The density of states (number of eigenvalues per site, per unit energy) for a one-, two-, five-, and ten-layer perfect wire with island concentration $p = 5\%$, calculated using the CPA. The energy E is expressed in terms of the off-diagonal H matrix elements V.

layers (i.e., normalize the density of states to the number of layers instead of to unity) and shift the origin of the bands (for the perfect case) to the same position (see Fig. 3) then the effect of islands on the wires with different numbers of layers can be easily compared. From Figs. 2 and 3 we see that when the number of layers in the wire is increased, the main effect on the DOS at the band edge is due to the different normalization factor. Looking at the subband representation [Eq. (8)], in each case channels (i.e., subbands) open one by one as the energy is increased. So in each case the same channels near the band edge are first opened with similar value for $\mathrm{Im}[g_i^{(\infty)}]$. The small difference in the height of peaks in Fig. 3 comes from different subband mixing due to disorder (see Ref. 13).

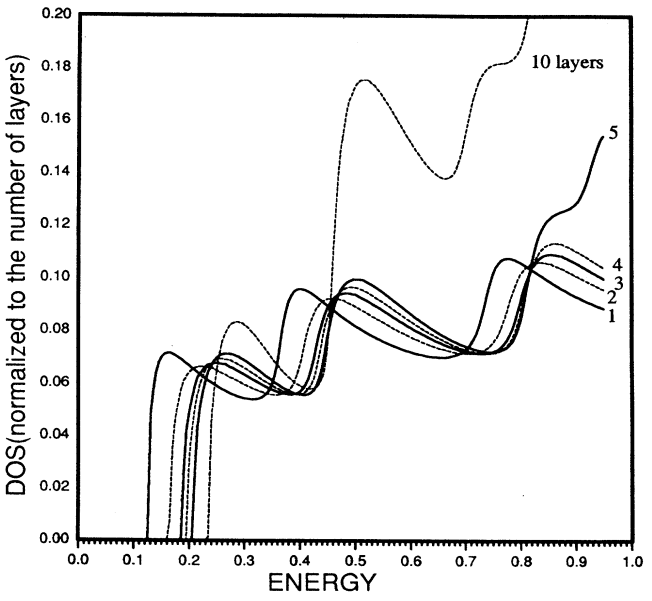

FIG. 3. The density of states (per site, per unit energy) multiplied by the number of layers in the wire, for the cases of one, two, three, four, five, and ten layers in the wire. The origin of the band is shifted to 0 in each case. The energy is in units of V.

Also, $\mathrm{Re}[\sigma(m)]$ increases as the number of layers increases, therefore the diagrams are shifting towards higher energies. This can be understood by comparison with Eq. (4): the Green's function in the denominator has the same normalization factor as the wave functions, which is the number of layers. Therefore, $\sigma(m)$ near the band edge increases with the number of layers. We conclude, therefore, that the best peak resolution, for a perfect wire with islands, is achieved in the case of a monolayer wire.

B. Real wires with or without islands

The term "real wire" refers here to any kind of quantum wire with uneven interfaces, i.e., rough edges. In order to determine the DOS, $\rho(E)$, of a real wire we have first calculated the integrated DOS

$$\mathcal{N}(E) = \int_{-\infty}^{E} \rho(E')dE'. \tag{10}$$

The integrated DOS of the system described by the Hamiltonian $\mathbf{H}$ is given by the number of negative eigenvalues of the characteristic matrix $\mathbf{C} = (\mathbf{H} - E\mathbf{I})$, where $\mathbf{I}$ is a unit matrix of the same order as $\mathbf{H}$. The numerical method used for the calculation of the integrated DOS was given by Evangelou.[18]

According to Ref. 18, for a real and symmetric block tridiagonal matrix $\mathbf{C}$, after transforming to upper triangular form by Gaussian elimination, the number of negative eigenvalues of $\mathbf{C}$ is equal to the number of negative diagonal elements of the reduced triangular matrix. Hence, the lower triangle of the matrix $\mathbf{C}$, for the Hamiltonian given by Eq. (1), has to be reduced to zero. Due to the nearest-neighbor character of the interactions only an $(M + 1) \times (M + 1)$ matrix needs to be stored during this calculation. This method allows very long quasi-one-dimensional systems to be considered. For the storage requirement of the algorithm the only important factor is the cross section, i.e., the number of sites in the slice $M = nl \times$ width (where nl is number of layers and *width* is the width of the system, i.e., "terrace" in our case). The integrated DOS is calculated by counting the negative diagonal elements generated by the elimination procedure. The DOS, $\rho(E)$, is obtained by differentiation which is performed simply by a finite-differences method: $\rho(E) = \Delta\mathcal{N}/\Delta E$, so that the DOS is represented as a histogram rather than a continuous line.

1. *Monolayer wires*

The DOS for real monolayer wires without and with islands [sections of wires given in Figs. 1(b) and 1(c)] are

given in Ref. 12, but only for energies close to the band edge. The whole energy range is given here, in Fig. 4 (diagrams are symmetric in respect to energy $E = 0$). Curve (a) in Fig. 4 corresponds to the wire with a constant width and without the islands, only meandering (fluctuations of the center of the wire) is included. This type of disorder has little effect on the spectrum, but the inclusion of width fluctuations [Fig. 4, curve (b)] severely degrades the peaks, leaving only the first subband distinct. The inclusion of islands in this structure wipes away even this remaining characteristic feature of the DOS [curve (c)].

The broadening and weakening of the peaks of the DOS, caused by the roughness of the boundaries of the wire, increases with increasing energy, i.e., the subband index. This is clearly shown in Ref. 13 on diagrams 4(a) and 4(b) where the DOS is given in each one-dimensional subband of the wire. A rough estimate for the change in the DOS ($\delta\rho_n$) in the subband n due to the width fluctuations (δw), is given by[13]

$$\delta\rho_n \sim -\, n\, \frac{a}{\langle w\rangle^2}\, \rho_n^3\ \delta w, \tag{11}$$

where a is the lattice constant and $\langle w\rangle$ is the average width of the wire. Relation (11) also suggests that peaks are more affected than flat parts (term ρ_n^3) and the effect decreases as average width of wire increases. If $\langle w\rangle$ is treated as an effective width of the wire "seen" by an electron on a length scale equal to the longitudinal wavelength of the electron λ, then this argument could be extended to the case of a meandering wire, when the width of each slice is the same.

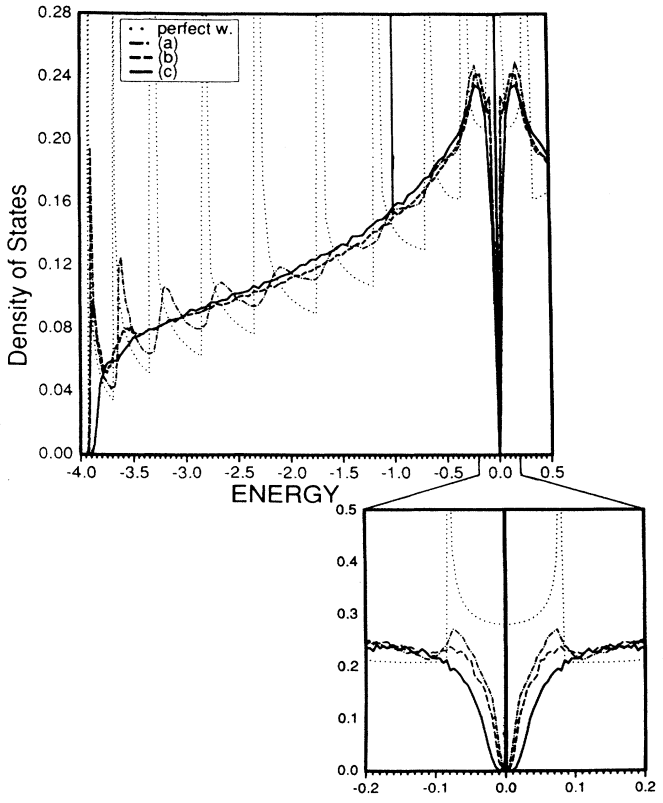

FIG. 4. The density of states (per site, per unit energy) for a monolayer wire, together with the perfect case (dotted line), corresponding to (a) only meandering wire; (b) wire in Fig. 1(b); (c) wire in Fig. 1(c). The lower diagram shows the region around energy $E = 0$ in more detail.

The DOS has a sharp dip with a very narrow gap in the center of the B subband (Fig. 4, lower diagram). There are also spikes in the DOS at the energies $E = 0$ (for all wires) and $E = \pm 1$ (noticeable only for wires with islands). These spikes, as well as the energy gap in the DOS diagram attracted special attention from Kirkpatrick and Eggarter.[10] They found that the tight-binding nearest-neighbor model for a substitutional alloy in the strong-scattering (i.e., band separation) limit gives rise to the following three different types of localized states.

(1) Localized states decaying exponentially (Anderson localization).

(2) States localized on small clusters of B atoms isolated by a boundary of A atoms.

(3) Kirkpatrick-Eggarter (KE) states: molecular states that, in practice, appear at special energies (e.g., $E = 0, \pm V$), localized partially by interference and partially by a physical boundary of A atoms. The wave function of these states is nonvanishing on only a finite number of sites and strictly zero elsewhere. Although it has been shown that, for the quantum percolation model, molecular states can be constructed arbitrarily close to any energy in the band,[19] the configurations supporting them are significantly less probable then those of $E = 0, \pm V$ and generally they will not be observed as spikes under numerical examination.

The spike at $E = 0$ for the wires without islands is solely due to type-3 localized states, because isolated B-atom clusters cannot appear. The inclusion of islands in the wire structure creates the possibility of type-2 states. A single isolated B atom (surrounded by A atoms) has a single eigenenergy zero and this state contributes to the spike at $E = 0$. A cluster of two B atoms surrounded by A atoms has two eigenstates, with energies $\pm V$, and these states will account for most ($\sim 95\%$) of the spike at $E = \pm 1$ in Fig. 4, curve (c). The rest of the states in this spike are KE states, while at the same energy type-1 states apparently coexist, unlike the case $E = 0$. This is important for the localization length (Sec. IV A). The probability of occurrence of other types of isolated clusters is so small, in our system, that they are not noticeable on the DOS diagram.

Our numerical calculations show that the DOS near the energy $E = 0$ appears to vanish, and this gap exists in all three cases (a), (b), and (c) in Fig. 4. The narrowing of the gap and the dip in the DOS diagram (Fig. 4, lower diagram) as the amount of disorder decreases is in agreement with the results of the quantum percolation problem,[20] where a concentration-dependent gap or depletion in the spectrum around the band center is observed. However, the form of the decay of the DOS immediately before (and after) the gap is fairly represented by the Lifshitz tail [$\rho(E) \sim \exp(-A|E|^{-3/2})$, where A

is a constant, see also Ref. 21]. This could suggest that the spectrum decays continuously to the energy $E = 0$ (which is forbidden[22] for the type-1 states).

2. *Wires with more than one layer*

We consider first the case of maximum correlation between the layers (i.e., identical layers). In this case, the DOS for the two-layer wire $[\rho_{2L}(E)]$, made up of two identical layers, is given by the DOS for a single layer of the wire [i.e., monolayer wire, $\rho_{1L}(E)$] by an expression of the form

$$\rho_{2L}(E) = \tfrac{1}{2}\left[\rho_{1L}(E-1) + \rho_{1L}(E+1)\right]. \tag{12}$$

The relation (12) can be generalized to the case of N layers

$$\rho_{NL}(E) = \frac{1}{N}\sum_{i=1}^{N} \rho_{1L}(E - E_i), \tag{13}$$

where the E_i are the lower subband edge energy shifts (due to quantization in the direction of growth of the new layers) given by

$$E_i = 2V\cos\left(\frac{i\pi}{N+1}\right), \qquad i = 1, \ldots, N. \tag{14}$$

This can be simply proven analytically using the following argument. Since the z component is separable, the band splits into subbands indexed by bound states in the z direction. Eigenstates of a single layer exist in each z subband but with a shifted eigenenergy [shifts are given by Eq. (14)]. Hence at the energy E exist all those N-layer states that correspond to the states in the monolayer wire with energy $E - E_i$ for which condition $|E - E_i| < 4V$ is satisfied. It should be possible to obtain the result (13) via the extension theory,[23] since in the case of identical layers the problem separates. Each state $|\Phi_E^{(i)}\rangle$ in an N-layer system can be constructed using only the single-layer states $|\psi_{E-E_i}\rangle$,

$$|\Phi_E^{(i)}\rangle = \frac{1}{\sqrt{N}} \begin{pmatrix} C_1^{(i)}|\psi_{E-E_i}\rangle \\ C_2^{(i)}|\psi_{E-E_i}\rangle \\ \vdots \\ C_N^{(i)}|\psi_{E-E_i}\rangle \end{pmatrix}. \tag{15}$$

The coefficients $(C_j^{(i)})^2$ give the probabilities of finding an electron in the jth layer. They can be determined from the Schrödinger equation for the N-layer system

$$\mathbf{H}^{(NL)}\,|\Phi_E^{(i)}\rangle = E\,|\Phi_E^{(i)}\rangle, \tag{16}$$

where $\mathbf{H}^{(NL)}$ has a block-tridiagonal form

$$\mathbf{H}^{(NL)} = \begin{pmatrix} \mathbf{H}^{(1L)} & \mathbf{V} & & & & & \\ \mathbf{V} & \mathbf{H}^{(1L)} & \mathbf{V} & & & & \\ & \mathbf{V} & \mathbf{H}^{(1L)} & \mathbf{V} & & & \\ & & & \ddots & & & \\ & & & & \ddots & & \\ & & & & \mathbf{V} & \mathbf{H}^{(1L)} \end{pmatrix}. \tag{17}$$

Note that in Eq. (17) the numbering of atoms is different from the numbering that is understood so far, i.e., instead of slice-by-slice order here it is layer-by-layer order since we wish to express $\mathbf{H}^{(NL)}$ in terms of $\mathbf{H}^{(1L)}$.

The relation (13) preserves the spikes and dips present in the monolayer structure, although shifted along the E axis. However, the gap in the DOS completely disappears for multilayer systems.

Next we consider the cases of *medium* and *zero* correlation between the layers of the wire. Figure 5 presents the density of states of a two-layer real wire, with islands, for all three considered degrees of correlation between the layers. As the structural correlation decreases, the DOS also decreases for energies close to the band edge. This is evident from Fig. 5, by comparing the region of energies $(-5, -4)$, where the number of states is decreasing, with the region $(-4, -3)$, where number of states is increasing. The example in Fig. 6 confirms this even more dramatically. Hence, the increase in the roughness of the lateral surface of the wire in the z direction causes migration of some states near the band edge towards higher energies.

The reason for this can be found by analyzing a cross section of these wires (see the inset to Fig. 6). The sides of the wire are rough and contain inlets. These inlets are not accessible to electrons with wavelengths longer than the size of the inlet. Therefore the states with the lowest energy, i.e., near the band edge, cannot be extended over the whole cross section of the wire, but only over the central region. This means that the effective width of wire for these states has been decreased (in the inset to Fig. 6 depicted by a broken line). The decrease of the wire width implies that the boundary roughness of wire has a stronger effect [according to the relation (11)] on

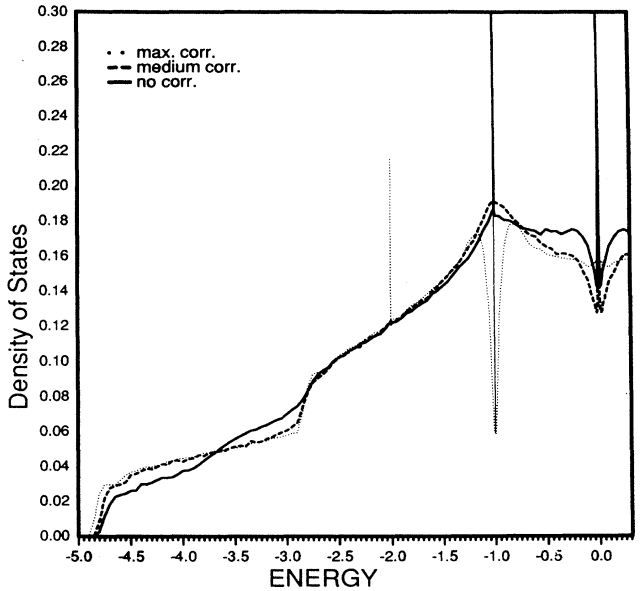

FIG. 5. The density of states (per site, per unit energy) for the two-layer real wire with islands, for zero correlation (full line), medium correlation (broken line), and maximum correlation (dotted line) between the layers. A section of a layer is given in Fig. 1(c).

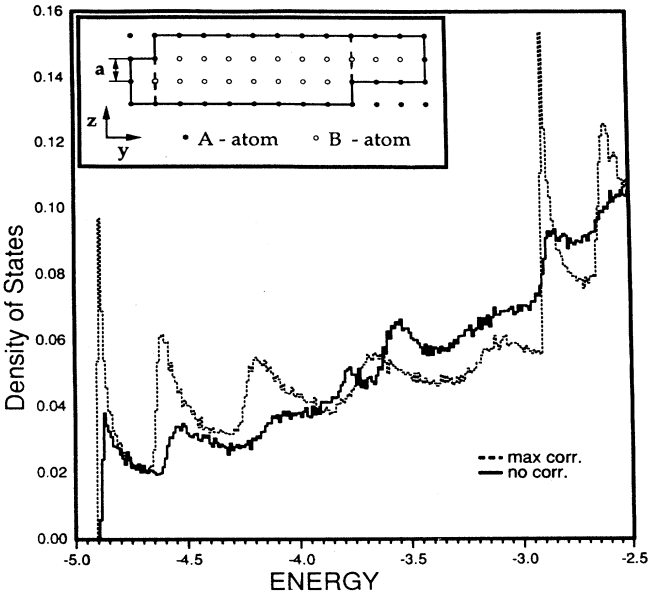

FIG. 6. The density of states (per site, per unit energy) for the two-layer wire, where each layer has a constant width and no islands, only the center of wire is fluctuating (meandering wire), for no correlation (full line) and maximum correlation (broken line) between the layers. The inset figure shows a cross section of the two-layer wire (not with maximum correlation between layers). Broken lines represent the effective size of the cross section for long-wavelength electrons.

the DOS, and also that the band edge is slightly shifted towards higher energies. Furthermore, this region of depleted density of states can be roughly estimated by comparing the transverse energy levels for the rectangular cross section of height $2a$ and $3a$. For the tight-binding model, the quantizations in the z direction are given by $E_z(h) = 2V\cos(i\pi a/h)$, where h is the height of the wire and $i = 1, ..., (h/a - 1)$. Hence the possible shifts in the energy are, for $h = 2a$, $E_z = 0$ and for $h = 3a$, $E_z = -1$. Therefore the energy of the state that extends over the parts of the wire with the height $h = 2a$ has to be at least $E_b + 1$, where E_b is the lower band-edge energy.

The dip in the DOS again appears around the center of the band ($E = 0$, Fig. 5), but there is no gap. Spikes are seen at $E = 0$ and $E = \pm 1$ for both cases.

From the previous discussion it is apparent that the addition of any new layer, which is not identical with the previous one, decreases the effective width of the wire for an electron with energy close to the band edge. This means further suppression of the subband structure for the DOS near the band edge. Also the density of states per site decreases due to different normalization factors (i.e., creation of new z subbands) when the number of layers increases. Hence the best peak resolution, for real wires, is achieved for monolayer structures.

IV. LOCALIZATION LENGTH

The process of wire generation gives a finite probability that the wire structure will be broken at some length. The existence of such breaks will drastically reduce the transport capabilities of the wire. In particular, for our electronic model it would lead to zero mobility. The quantum wire structures considered here are such that, in a classical connectivity sense, they remain connected over very long distances (more than 10^4 slices). However, the fact that the structure is extended does not imply that the electronic states supported on it will also be extended.

Johnston and Kunz[24] rigorously proved that the elements of the transmission matrix for a very long disordered wire show asymptotic exponential decrease with the length of the system. The exponent is the smallest Lyapunov exponent (γ_1) associated with the system, multiplied by the length of wire. This means that all states are at least exponentially localized in our real quantum wire system. The localization length (λ) is equal to the inverse of the smallest Lyapunov exponent ($\lambda = 1/\gamma_1$) and determines the transmission probability T of a quasi-one-dimensional disordered system of length L by $T = \exp(-2L/\lambda)$. Hence, the quantum-mechanical connectivity of a wire is defined by the localization length.

It was also proved (Ref. 25) that for each of the elements $(\mathbf{G}^{(L)}_{1,L})_{i,j}$ of the submatrix $\mathbf{G}^{(L)}_{1,L}$ of the Green's function

$$\lim_{L\to\infty} \frac{1}{L} \ln |[\mathbf{G}^{(L)}_{1,L}(E + i0^+)]_{i,j}| = -\frac{1}{\lambda(E)} . \tag{18}$$

$\mathbf{G}^{(L)}_{1,L}$ couples pairs (i,j) of sites at opposite ends of a bar of length L. It can be calculated using the Green's function iterative method[15,14,16]

$$\mathbf{G}^{(L+1)}_{1,L+1} = \mathbf{G}^{(L)}_{1,L}\mathbf{V}^{\dagger}_{L,L+1}\mathbf{G}^{(L+1)}_{L+1,L+1} , \tag{19a}$$

$$\mathbf{G}^{(L+1)}_{L+1,L+1} = [E\mathbf{I} - \mathbf{H}^{(1)}_{L+1} - \mathbf{V}_{L+1,L}\mathbf{G}^{(L)}_{L,L}\mathbf{V}^{\dagger}_{L,L+1}]^{-1} . \tag{19b}$$

This method uses quasi-one-dimensional geometry to perform iterative calculations by successively adding slices to the end of the bar, as in the integrated DOS calculations. This numerical technique has proved very reliable for the Anderson localization problem.[26]

According to Eq. (18) λ is the decay length for the amplitude of $\mathbf{G}^{(L)}_{1,L}$. The equation that is usually used for calculations of localization length is

$$\frac{2}{\lambda} = -\lim_{L\to\infty} \frac{1}{L} \ln \mathrm{Tr} |\mathbf{G}^{\dagger(L)}_{1,1}\mathbf{G}^{(L)}_{1,L}| . \tag{20}$$

λ is a self-averaging quantity (Ref. 25) and, in practice, the statistical accuracy of λ can be controlled by its relative error, which is empirically given by (see Refs. 14, 27, and 28)

$$\epsilon^2 \simeq \frac{2\lambda}{L} \tag{21}$$

for fixed cross section M. Note that the error depends on the value for the localization length.

A. Monolayer quantum wires

The results for the localization length as a function of energy for the monolayer real wire with/without islands are given in Fig. 7. Values for λ were calculated using systems of 10^5 slices, which means a maximum error of $\sim 4\%$ in Fig. 7(a) (no islands), and $\sim 2.5\%$ maximum error in Fig. 7(b) (with islands). Apart from the peak near the band edge, interface disorder alone is sufficient to localize all of the states to within ~ 70 lattice spacings. The addition of islands has a strong influence on the localization length near the band edge and further reduces λ to the maximum of ~ 35 lattice spacings.

In order to get a better understanding of the peak in case (a) we have presented the DOS for the same case in Fig. 7. It is apparent that the localization length peak appears at the same energy where the DOS has a local minimum. Also, the following local minimum in the localization length corresponds exactly to the small peak in the DOS, which is the last remaining feature from the subband inverse square-root singularities. This "inverse" DOS characteristic for the energy dependence of the localization length of a quantum wire can be explained by a phase-space argument: the scattering cross section of the electron is proportional to the number of available states into which it can be scattered by disorder.[29] This is clearly evident from Figs. 8(a) and 8(b), where we have results near the band edge for a meandering wire and a perfect wire with island concentration $p = 1\%$, respectively. The energy dependence of the DOS and λ in these two examples show almost completely opposite trends: a strong reduction in the localization length when the DOS is increasing (i.e., when a new subband emerges) and then an increase in the localization length while the DOS goes down. However, when KE states (see Sec. III B) are dominant, i.e., at $E = 0$ (Fig. 4), this relationship in trends is not so local on the energy scale.

The localization length decreases abruptly around the B-subband center (Fig. 7). At the subband center ($E = 0$) it is reduced to a single lattice spacing. Very strong localization at the center of the B subband is also reported elsewhere.[20,30] For this energy, in the extreme split-band limit, no Anderson localized states are observed,[10,20] but only type-2 and type-3 states exist. Type-2 states are obviously isolated single atoms, but type-3 (KE) states extend over an unspecified length, which cannot be de-

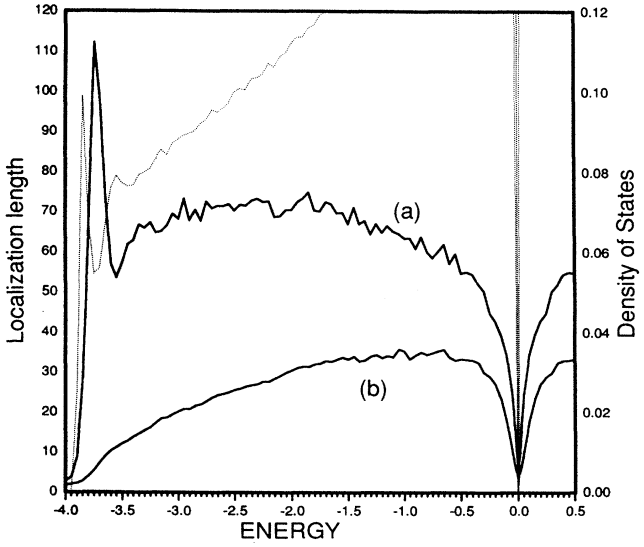

FIG. 7. The localization length (in units of lattice spacing a) as a function of energy (diagrams are symmetric in respect to $E = 0$) for the real, width ten wires: (a) without islands [section of wire given in Fig. 1(b)], (b) with islands, concentration $p = 5\%$ [section given in Fig. 1(c)]. DOS for the case (a) is given as well (dotted line). The energy is in units of V.

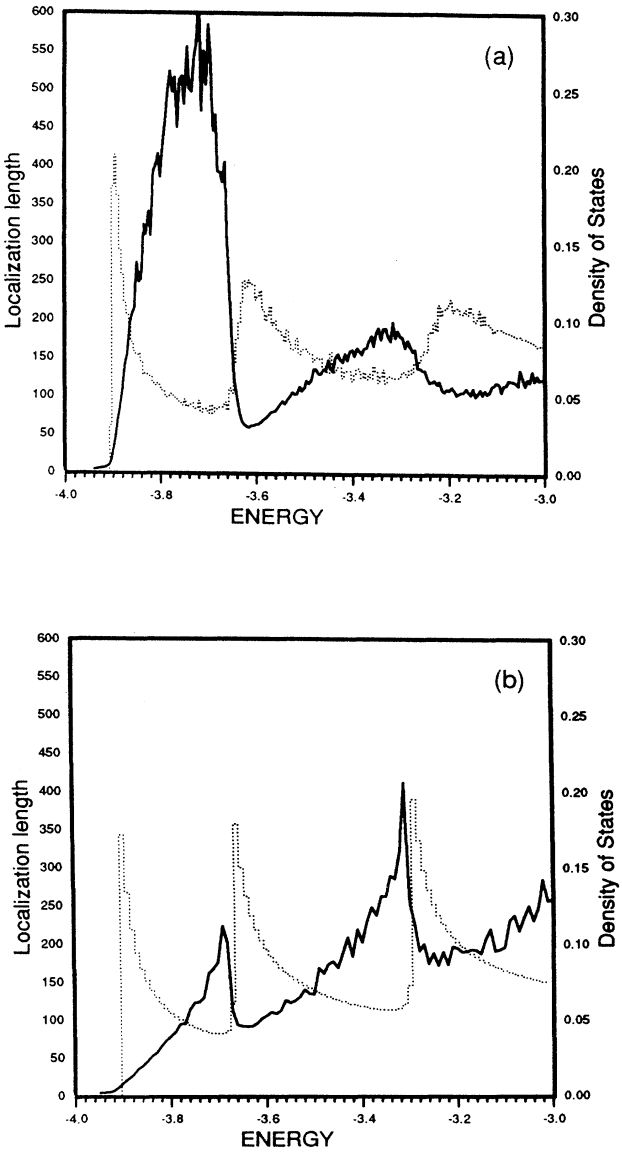

FIG. 8. The localization length (full line) and the density of states (dotted line) for energies near the band edge for a monolayer: (a) meandering wire (width of each slice is constant and equal to ten lattice spacings, no islands, only center of wire is fluctuating), and (b) a perfect wire with islands, concentration of islands $p = 1\%$.

termined using our Green's-function method [Eq. (20)]. The KE states behave like traps for electrons and, since there are no current-carrying states in the gap, the localization length (which is now transmission probability) is strongly reduced. Furthermore, it seems that the influence of these states is not strictly limited to $E = 0$. Since states close to $E = 0$ must be similar to KE states but also orthogonal to them, the KE states behave as extra scatterers of an electron. Thus the presence of the KE states acts to reduce the elastic mean free path for electrons with energies close to $E = 0$, and therefore to reduce the localization length.

B. Multilayer quantum wires

Here we are dealing mainly with the two-layer systems. Results for this type of system lead us to conclusions which can be extended to systems with more than two layers. The localization length for the two-layer real wire without islands is given in Fig. 9 for the three typical correlation functions between the layers. Figure 10 presents results for the same wire but with islands.

Results for the case of two identical layers (maximum correlation) look unexpected at first glance: the maximum value of the localization length for the two-layer wire does not exceed the maximum localization length in a single layer. Furthermore, the localization length for the system of two identical layers, $\lambda_{2L}(E)$, can be expressed in terms of $\lambda_{1L}(E)$ for a single layer by the relation

$$\lambda_{2L}(E) = \max\{\lambda_{1L}(E-1), \lambda_{1L}(E+1)\}. \tag{22}$$

The validity of Eq. (22) can be checked in Fig. 11, but also

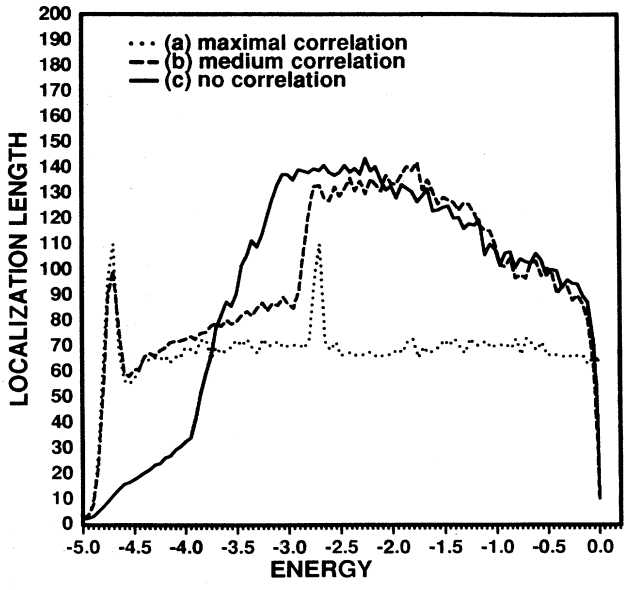

FIG. 9. The localization length (in units of lattice spacing a) as a function of energy (in units of V) for a two-layer structure without islands, layers have the same disorder parameters, and the correlation between them is (a) maximum, (b) medium, (c) no correlation.

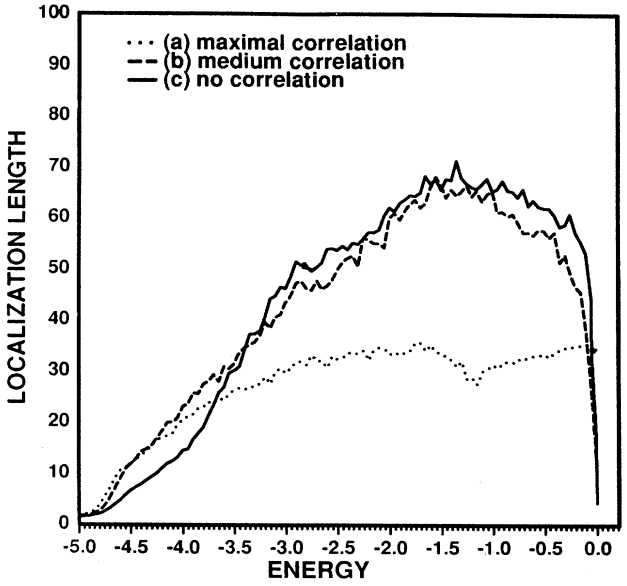

FIG. 10. As in Fig. 9, but for a wire with islands.

proved analytically. However, we shall first generalize Eq. (22) to the case of N layers,

$$\lambda_{NL}(E) = \max\{\lambda_{1L}(E-E_1), \lambda_{1L}(E-E_2), \ldots, \lambda_{1L}(E-E_N)\}, \tag{23}$$

where E_i are the subband energies given by Eq. (14). Previously we have seen that, when the problem separates, in the N-layer system exist only states $|\Phi_E^{(i)}\rangle$ which depend solely on a single-layer state $|\psi_{E-E_i}\rangle$ [Eq. (15)]. The state $|\psi_{E-E_i}\rangle$ is a type-1 state (Anderson localiza-

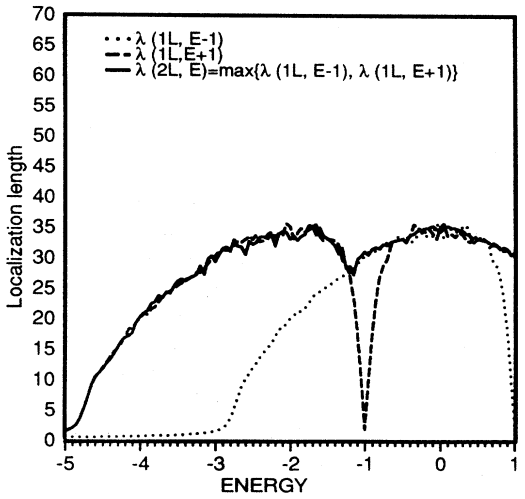

FIG. 11. The localization length (in units of lattice spacing a) as a function of energy (in units of V) for a two-layer wire with islands (as in Fig. 10 maximum correlation case, here full line) along with the localization lengths for a monolayer wire, but shifted for $+1$ (dotted line) and -1 (broken line) along the energy axis. Within the error-bar relationship between these quantities [Eq. (22)] is correct.

tion) and therefore its amplitude is dominated by the factor

$$|\psi_{E-E_i}(r)| \sim \exp\left(-\frac{r}{\lambda(E-E_i)}\right). \quad (24)$$

Hence the N-layer state $|\Phi_E^{(i)}\rangle$ also has a localization length $\lambda(E-E_i)$. Now, in an N-layer system at energy E, the states $|\Phi_E^{(i)}\rangle$ define a set of Lyapunov exponents associated with individual z subbands. The localization length of an electron at energy E is determined by the smallest Lyapunov exponent, which means the largest $\lambda_{1L}(E-E_i)$ $(i=1,\ldots,j\leq N)$. This is expressed by Eq. (23).

The first consequence of Eq. (23) has already been mentioned: by adding identical layers to the quantum wire, the localization length, and therefore the transport properties, cannot be improved, despite the creation of additional space for electron movement. There is no mixing between the subbands created by adding new layers and hence the additional space does not become available. Does that, paradoxically, mean that the creation of disorder in the z direction gives rise to longer localization lengths? The diagram in Fig. 9 gives us an answer (this case is more transparent than in Fig. 10 because it excludes effects due to islands). These diagrams have three characteristic parts, roughly the following: (i) between -5 and -4, (ii) between -4 and -3, and (iii) between -3 and 0. Now case (b) (medium correlated layers) gives a similar λ to case (a) (maximum correlation) for small energies [region (i)], while it is more similar to case (c) (no correlation) for higher energies [region (iii)]. For small energies the electron wavelength is relatively large and therefore less sensitive to the small-scale edge roughness. Hence, if structural fluctuations over long lengths are dominant, then cases (b) and (a) are similar. On the other hand, for higher energies and smaller wavelengths short-scale disorder dominates, and hence case (b) is more like case (c). Part (ii) is a transition region, where disorder-induced mixing of z subbands gives rise to an increase of the localization length. The same explanations are also valid for Fig. 10. Islands have a stronger impact for smaller energies and they also cause stronger z-subband mixing between the region of mainly one z subband [part (i)] and two z subbands [part (iii)].

Comparing the results for monolayer and double-layer quantum wires one can say that by increasing the number of layers in the wire the localization length can be increased, but not uniformly over the whole energy band. Near the band edge it is difficult to achieve longer λ than for the monolayer wire. This is the region of energies, like part (i) in Figs. 9 and 10, where the wire is effectively narrower for electrons due to the long electron wavelength. This region shrinks when the average width of a layer increases but expands when the number of layers increases, because the wave function nodes in the z direction can only be fitted into the central part of a cross section. Beyond these energies, as the Fermi energy increases the localization length also grows, with a gradient which increases monotonically with disorder. This increase of λ with energy saturates when all of the z subbands are involved. It seems that the maximum value for λ is linearly proportional to the number of layers (we have checked this for few energy points). This is consistent with the well-known behavior of electrons in the quasi-one-dimensional systems far from the metal-insulator transition,[14] and can be understood in terms of the fluctuations of the average potential seen by an electron. Also this is in agreement with the well-known approximative relation for the localization length: $\lambda = Nl_{\rm el}$, where N is the number of occupied subbands (which is proportional to the number of layers) and $l_{\rm el}$ is the elastic scattering length. Hence the upper limit for the localization length is determined by the disorder in a layer.

The edge fluctuations along the wire, $\delta y(x)$, determine the upper limit for λ, while the edge fluctuations in a cross section, $\delta y(z)$, further modulate the shape of the $\lambda(E)$ diagram. We can conclude, therefore, that the localization length in structurally disordered quantum wires is predominantly limited by the disorder along the wire.

V. CONCLUSION

We have obtained DOS and localization length plots as a function of the energy E for compositionally disordered quantum wires. The disorder in the wire is generated using concrete simulations of vicinal surface-grown quantum wires. Results for the DOS of monolayer real wires with islands show strong suppression of the sharp subband features of ideal quasi-one-dimensional systems. All states are localized within a few tens of lattice spacings. This implies a very low mobility for these structures, contrary to the predicted high mobility for perfect quantum wires. The case of quantum wires without islands is more promising. Since the states near the band edge are less affected by interface roughness than those elsewhere in the spectrum, the first few subbands are observed in the DOS spectra as well-distinguished features. The localization length is at least doubled right across the band, with a sharp peak in the first subband.

Studies that go beyond monolayer structures show that the increase in the number of layers does not necessarily result in an improvement of the above-mentioned electronic characteristics. Firstly, the results depend on the correlations between the layers. The DOS for any multilayer structure cannot produce better resolution of the subband peaks (rounded and broadened due to disorder) than in the monolayer case. Localization lengths do increase with the addition of new layers, but actual values for this quantity depend on the energy and on the correlations between the layers. It seems that the maximum localization length is proportional to the number of layers, although near the band-edge uncorrelated layers produce smaller localization lengths than monolayer structures.

Some other fabrication techniques usually produce wider quantum wires and, therefore, these results are

less applicable, since the influence of edge disorder decays as the width of the wire increases. Nevertheless, the ultimate aim of reducing device size as much as possible justifies work in the domain of very narrow quantum wires.

ACKNOWLEDGMENTS

One of us (K.N.) wishes to thank the CVCP of the Universities of the United Kingdom for financial support.

[1] J. H. Neave, P. J. Dobson, B. A. Joyce, and J. Zhang, Appl. Phys. Lett. **47**, 100 (1985).
[2] P. M. Petroff, A. C. Gossard, and W. Weigmann, Appl. Phys. Lett. **45**, 620 (1984).
[3] K. J. Hugill, S. Clarke, D. D. Vvedensky, and B. A. Joyce, J. Appl. Phys. **66**, 3415 (1989).
[4] A. Myers-Beaghton, J. P. G. Taylor, D. D. Vvedensky, K. J. Hugill, and A. MacKinnon, J. Cryst. Growth **111**, 328 (1991).
[5] H. Sakaki, Jpn. J. Appl. Phys. **19**, 94 (1980).
[6] Y. Arakawa and H. Sakaki, Appl. Phys. Lett. **40**, 939 (1982).
[7] T. Fukui and H. Saito, Appl. Phys. Lett. **50**, 824 (1987).
[8] M. Tsuchiya, J. M. Gaines, R. H. Yan, R. J. Simes, P. O. Holtz, L. A. Coldren, and P. M. Petroff, Phys. Rev. Lett. **62**, 466 (1989).
[9] C. Weisbuch, R. Dingle, A. C. Gossard, and W. Wiegmann, J. Vac. Sci. Technol. **17**, 1128 (1980); R. S. Miller, W. Tsang, and O. Munteanu, Appl. Phys. Lett. **41**, 374 (1982).
[10] S. Kirkpatrick and T. P. Eggarter, Phys. Rev. B **6**, 3598 (1972).
[11] D. J. Thouless, J. Phys. C **4**, L92 (1971).
[12] J. P. G. Taylor, K. J. Hugill, D. D. Vvedensky, and A. MacKinnon, Phys. Rev. Lett. **67**, 2359 (1991); J. P. G. Taylor, Ph.D. thesis, Imperial College of Science, Technology and Medicine, London, 1990.
[13] K. Nikolić and A. MacKinnon, J. Phys. Condens. Matter **4**, 2565 (1992).
[14] A. MacKinnon and B. Kramer, Z. Phys. B **53**, 1 (1983).
[15] A. MacKinnon, Z. Phys. B **59**, 385 (1985).
[16] P. A. Lee and D. S. Fisher, Phys. Rev. Lett. **47**, 882 (1981); D. J. Thouless and S. Kirkpatrick, J. Phys. C **14**, 235 (1981).
[17] R. J. Elliot, J. A. Krumhansl, and P. L. Leath, Rev. Mod. Phys. **46**, 465 (1974).
[18] S. N. Evangelou, J. Phys. C **19**, 4291 (1986).
[19] J. T. Chayes, L. Chayes, J. R. Franz, J. Sethna, and S. A. Trugman, J. Phys. A **19**, L1173 (1986).
[20] C. M. Soukoulis, E. N. Economou, and G. S. Grest, Phys. Rev. B **36**, 8649 (1987).
[21] J. E. Gubernaitis and P. L. Taylor, J. Phys. C **4**, L94 (1971).
[22] R. E. Borland, Proc. Phys. Soc. **78**, 926 (1961); P. L. Taylor, *ibid.* **88**, 753 (1966); H. Matsuda, Prog. Theor. Phys. **38**, 512 (1967).
[23] W. A. Schwalm and M. K. Schwalm, Phys. Rev. B **37**, 9524 (1988).
[24] R. Johnston and H. Kunz, J. Phys. C **16**, 3895 (1983).
[25] R. Johnston and H. Kunz, J. Phys. C **16**, 4565 (1983).
[26] C. M. Soukoulis, I. Webman, G. S. Grest, and E. N. Economou, Phys. Rev. B **26**, 1838 (1982); A. D. Zdetsis, C. M. Soukoulis, E. N. Economou, and G. S. Grest, *ibid.* **32**, 8711 (1986).
[27] A. MacKinnon and B. Kramer, Phys. Rev. Lett. **47**, 1546 (1983).
[28] J. Sak and B. Kramer, Phys. Rev. B **24**, 1761 (1983).
[29] J. Masek and B. Kramer, J. Phys. Condens. Matter **1**, 6395 (1989).
[30] Y. Shapir, A. Aharony, and A. B. Harris, Phys. Rev. Lett. **49**, 486 (1982).